A SnS_2 Molecular Precursor for Conformal Nanostructured Coatings

Yong Zuo[a,b], Junshan Li[a,b], Xiaoting Yu[a,b], Ruifeng Du[a,b], Ting Zhang[c], Xiang Wang[a,b], Jordi Arbiol[c,d], Jordi Llorca[e], and Andreu Cabot [a,d,*]

[a] Catalonia Institute for Energy Research - IREC, Sant Adrià del Besòs, Barcelona 08930, Spain

[b] Departament d'Enginyeria Electrònica i Biomèdica, Universitat de Barcelona, Barcelona 08028, Spain

[c] Catalan Institute of Nanoscience and Nanotechnology (ICN2), CSIC and BIST, Campus UAB, Bellaterra, 08193 Barcelona, Spain

[d] ICREA, Pg. Lluís Companys 23, 08010 Barcelona, Spain

[e] Institute of Energy Technologies, Department of Chemical Engineering and Barcelona Research Center in Multiscale Science and Engineering, Universitat Politècnica de Catalunya, EEBE, 08019 Barcelona, Spain

ABSTRACT: We present a simple, versatile and scalable procedure to produce SnS_2 nanostructured layers based on an amine/thiol-based molecular ink. The ratios amine/thiol and Sn/S, and the reaction conditions are systematically investigated to produce phase-pure SnS_2 planar and conformal layers with a tremella-like SnS_2 morphology. Such nanostructured layers are characterized by excellent photocurrent densities. The same strategy can be used to produce SnS_2-graphene composites by simply introducing graphene oxide (GO) into the initial solution. Conveniently, the solvent mixture is able to simultaneously dissolve the Sn and Se powders and reduce the GO. Besides, $SnS_{2-x}Se_x$ ternary coatings and phase pure $SnSe_2$ can be easily produced by simply incorporating proper amounts of Se into the initial ink formulation. Finally, the potential of this precursor ink to produce gram scale amounts of unsupported SnS_2 is investigated.

INTRODUCTION

The production of planar and conformal nanostructured layers with high surface areas and porosity using simple, rapid, cost-effective and scalable processes that are neither energy nor labor intensive is a topic of major relevance.[1–3] Toward this goal, solution-based strategies based on the decomposition, assembly and/or deposition of salts, molecular precursors or colloidal nanoparticles offer obvious advantages over physical and chemical vacuum-based technologies.[4] However, the use of salts generally leads to the incorporation of large amounts of impurities in the final material and may result in inhomogeneous layer compositions. Besides, nanoparticle-based inks suffer from suspension stability and result in layers characterized by inadequate interphases with the support, with poor charge transfer and feeble mechanical stability, *i.e.* present delamination issues.[5–11] On the other hand, molecular precursors generally provide a homogeneous mixing of the precursor elements that ensures a uniform layer composition without impurities. Additionally, the crystallization of the material post deposition can considerably improve charge transfer/transport properties and layer adherence.[2]

In 2004, Mitzi and coworkers reported the use of hydrazine to produce a molecular ink from the dissolution of bulk SnS_2 and $SnSe_2$ in the presence of excess elemental chalcogen.[12] The process was facilitated by the *in-situ* reduction of the elemental chalcogen to produce chalcogenide anions that subsequently started a series of nucleophilic reactions with the bulk chalcogenide, breaking it down to eventually yield soluble molecular metal chalcogenide species.[12] The obtained molecular inks could then be spin-coated and thermally annealed at 350 °C to yield phase-pure $SnS_{2-x}Se_x$ thin films with high charge carrier mobility.[12] After this pioneer report, the hydrazine route was demonstrated effective in producing a plethora of chalcogenides, including $GeSe_2$,[13] $Cu_{1.9}S$,[14] In_2Se_3,[15] ZnTe,[16] In_2Te_3,[17] GeSbSe[18], $CuInSe_2$[19], and $CuInTe_2$[17]. The use of hydrazine finds advantages on its high reduction power, small size, volatility and on leaving no carbon residue. However, hydrazine is highly toxic and explosive, thus it is not convenient for scale-up and commercial applications.[20]

To avoid the disadvantages of hydrazine, the Brutchey group demonstrated a binary solvent mixture based on ethanedithiol (Edt) and ethylenediamine (En), named the ¨alkahest solvent¨, to dissolve and recover several V_2VI_3 chalcogenides, including As_2S_3, As_2Se_3, As_2Te_3, Sb_2S_3, Sb_2Se_3, Sb_2Te_3, Bi_2S_3, Bi_2Se_3 and Bi_2Te_3,[21] at room temperature and ambient pressure, under air atmosphere and in just few minutes.[21,22] This amine-thiol solution system dissolves the bulk chalcogen through an amine-catalyzed reaction resulting in alkyl di-, tri-, and tetrachalcogens while -SR species bind to the metal ions.[20,21,23] Various combinations of mono- or dithiols with primary mono- and/or diamines,

as well as different amine/thiol ratios have been used to dissolve a plethora of metal and chalcogen precursor materials[20,24,25]. As an example, Cu, Zn, Sn, and In are soluble in butylamine and Edt;[26] M_aX_n (M = Cu^+, Cu^{2+}, Zn^{2+}, Sn^{2+}, In^{3+}, Ga^{3+}; X = Cl^-, $acac^-$, OAc^-, O^{2-}) can be easily dissolved in a mixture of hexylamine and propanethiol; and M_bY_n (M = Cu^+, Cu^{2+}, Sn^{2+}, In^{3+}; Y = S^{2-}, Se^{2-}) are highly soluble in hexylamine and Edt.[27] In the amine-thiol system, the main difficulty to prepare a phase pure material is to find the proper amine and thiol mixture, their ratio and reaction conditions to crystallize the targeted product in the desired phase, preventing the formation of unwanted secondary phases.

SnS_2 is an indirect n-type semiconductor that is attracting significant interest as absorber material for solar energy conversion due to the abundance of its constituting elements and its excellent optoelectronic properties in part related to its layered structure. To prepare SnS_2 different methods have been put forward, including hydrothermal,[28–30] hot-injection,[31–33] heat-up,[34,35] exfoliation,[36–38] and chemical vapor deposition.[39–41] Sn has been also dissolved in 10/1 of En/Edt to recover SnS,[42] but the production of pure SnS_2 by this method has been so far elusive.

Herein, we present a simple route based on a molecular ink to produce phase pure SnS_2 from a Edt and En mixture. The ratio of Sn/S, En/Edt and the annealing process are investigated to define the optimal conditions to recover pure SnS_2 planar and conformal layers. We additionally study the production of ternary $SnS_{2-x}Se_x$ and phase pure $SnSe_2$, the one step production of composite of SnS_2/reduced graphene oxide (SnS_2/rGO) composites and the photocatalytic properties of the produced layers.

RESULTS AND DISCUSSION

In our first attempts to produce SnS_2, stoichiometric molar amounts of sulfur and tin powders (Sn/S=1/2) were dissolved in a volume ratio En/Edt=10/1 at 70 ºC for 1h to obtain an optically clear pale yellow solution. The precursor ink was coated onto a glass substrate and the obtained film was annealed at 320 °C for 30 min. Upon annealing, the layer turned grey yellow. Scanning electron microscope (SEM) characterization showed the layer to contain a large density of quasi-spherical flower-like structures (Figure 1a), but powder X-ray diffraction (XRD) analysis identified the main crystal phase of the obtained material as SnS (Figure 1b), with only a minor amount of SnS_2 (Figure 1b).

The precursor solution was modified by incorporating an additional amount of sulfur (Sn/S=1/3) to correct for the low quantity of this element in the final layer. This precursor solution displayed a much more intense yellow color (Figure 1c). XRD analyses of the layers produced from the coating and posterior annealing of this precursor ink showed a notable increase of the amount of SnS_2, but SnS impurity peaks were still evident. Besides, the structure of the obtained film changed from the quasi-spherical flowers to tremella-like particles (Figure 1d). Similar results were obtained when instead of increasing the amount of sulfur, we decreased the concentration of Edt in the initial solution (Sn/S=1/2; En/Edt=20/1). This precursor solution decomposed into tremella-like structures with a main SnS_2 phase and a residual SnS component (Figure 1b,e).

To further adjust the stoichiometry and crystal phase of the final layer, we simultaneously increased the amount of sulfur (Sn/S=1/3) and reduced the amount of Edt (En/Edt=20/1). Using this new precursor solution (Sn/S=1/3, En/Edt=20/1), which displayed a green color (Figure 1c), phase-pure tremella-like SnS_2 could be finally recovered (Figure 1b,f). Energy dispersive X-ray spectroscopy (EDX) analysis further confirmed the composition of the obtained layer to be consistent with stoichiometric SnS_2 (Table S1).

Generally, lower amounts of Edt favored the formation of the SnS_2 phase over SnS. Pure SnS_2 could be obtained with Edt contents of En/Edt=20/1 or lower when using an excess of S, Sn/S≤1/3 (Figures 2a and S1). However, without Edt, the Sn and S powder mixture could not be fully dissolved (Figure 2b, S1) and no SnS_2 could be recovered. On the amine side, replacing En by hexylamine or butylamine did not allow the dissolution of proper amounts of Sn and S (Figure S2).

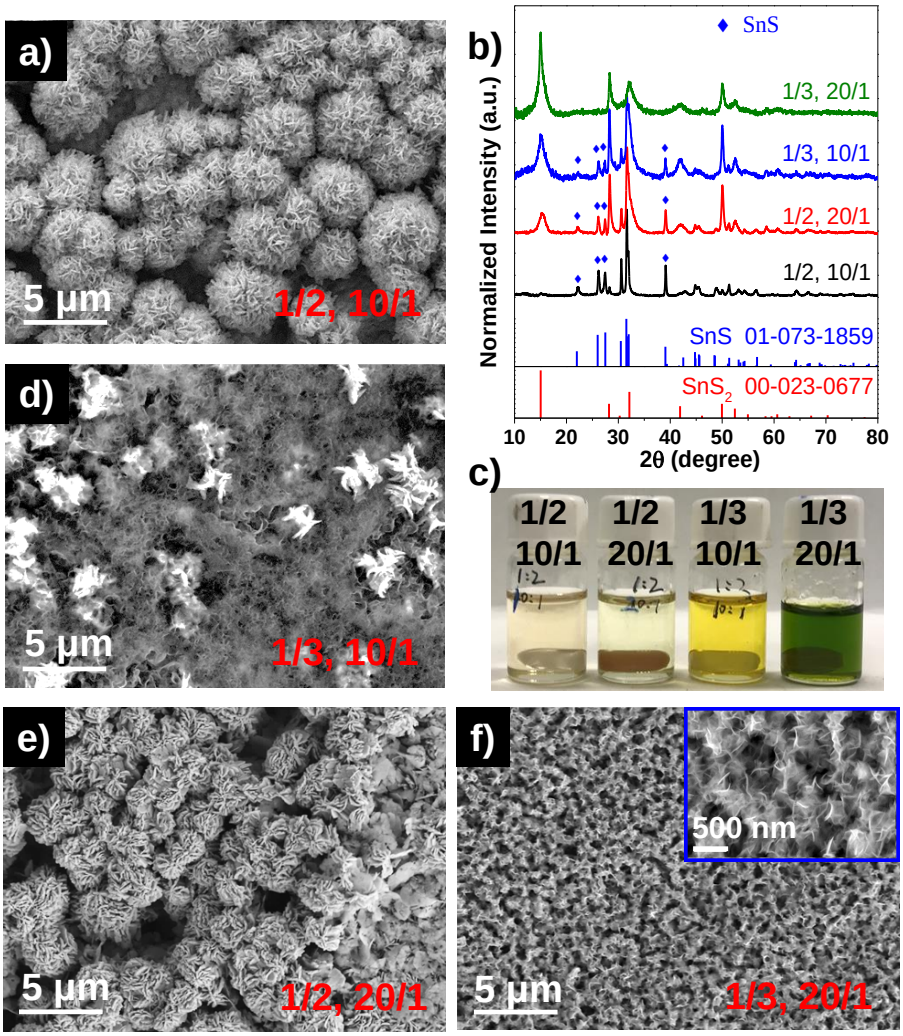

Figure 1. a) SEM micrograph of the material recovered after annealing a layer produced from an ink containing a molar ratio Sn/S=1/2 and a volume ratio En/Edt=10/1. b) XRD patterns of materials obtained after annealing layers produced from inks containing different Sn/S (1/2 or 1/3) and En/Edt ratios (10/1 or 20/1), as specified. c) Optical photographs of molecular inks obtained by dissolving different Sn/S (1/2 or 1/3) and En/Edt ratios (10/1 or 20/1), as specified. d-f) SEM micrographs of materials obtained after annealing layers produced from different Sn/S (1/2 or 1/3) and En/Edt ratios (10/1 or 20/1), as specified. Inks were formulated by dissolving the proper Sn and S ratios in En/Edt mixtures at 70 ºC for 1 h. Annealing conditions: 320 ºC, 30 min.

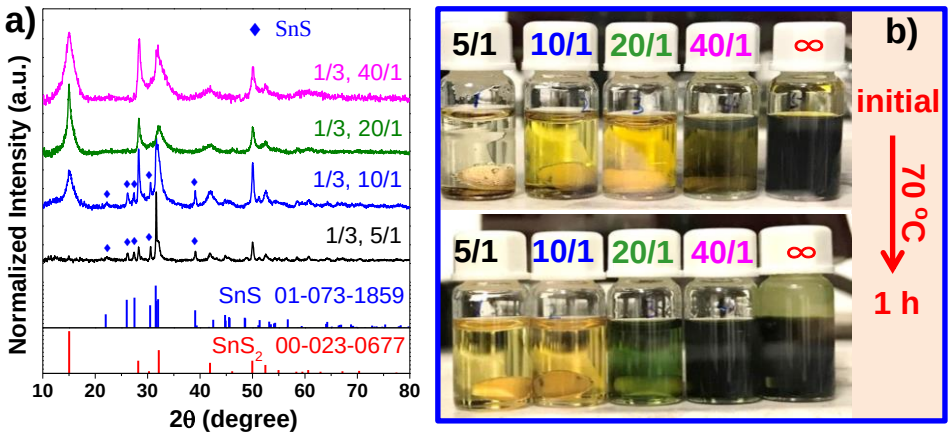

Figure 2. a) XRD patterns of sample recovered after annealing layers produced from inks containing different ratios En/Edt (from 5/1 to 40/1), as specified b) Optical photographs of SnS_2 molecular inks prepared with different ratios En/Edt (from 5/1 to 40/1) before and after heating at 70 °C for 1 h, as specified. Ink formulation parameters: Sn/S=1/3, 70 ºC, 1 h. Annealing conditions: 320 ºC, 30 min.

The higher the Edt concentration, the lower the time required to obtain an optically clear ink (Table S2). When using dissolution times in the range between 20 min and 1 h, no major effect was observed on the phase and structure of the produced material. However, when increasing the dissolution time, the SnS phase appeared even when using the previously defined as proper precursor compositions: Sn/S=1/3, En/Edt=20/1 (Figure 3a). EDX analysis further confirmed the Sn/S ratio of the annealed material to increase with the time of preparation of the precursor solution (Table S3). Additionally, the color of the ink also faded with the dissolution time (Figure 3b). Besides, the morphology of the final material turned toward sunflower-like structures when dissolution time increased to 3 h and above (Figure S3). We hypothesize that all these observations were associated with a sulfur loss during ink formulation. This loss was in the form of H_2S that was produced by the reaction of elemental sulfur with amine,[43,44] To prove this hypothesis, we added an additional amount (0.5 mmol) of sulfur powder into a SnS_2 molecular ink after 6 h at 70 ºC. This ink was mixed for additional 30 min to dissolve the added sulfur. After this time, the intense green color was recovered, and pure SnS_2 phase with a tremella morphology was obtained after annealing (Figure S4).

When applying no heat, a suitable ink could be prepared by dissolving proper amounts of Sn and S (Sn/S=1/3) in En/Edt=20/1 at ambient temperature for 6 h. In this condition, no significant loss of sulfur was detected and pure SnS_2 could be recovered after annealing (Figure S5). Overall, to optimize time and ensure a proper product phase with tremella like morphology (Figure 3a,c), we fixed the ink preparation time at 30 min, dissolution temperature at 70 ºC, the element ratio at Sn/S=1/3 and the solvent ratio at En/Edt=20/1.

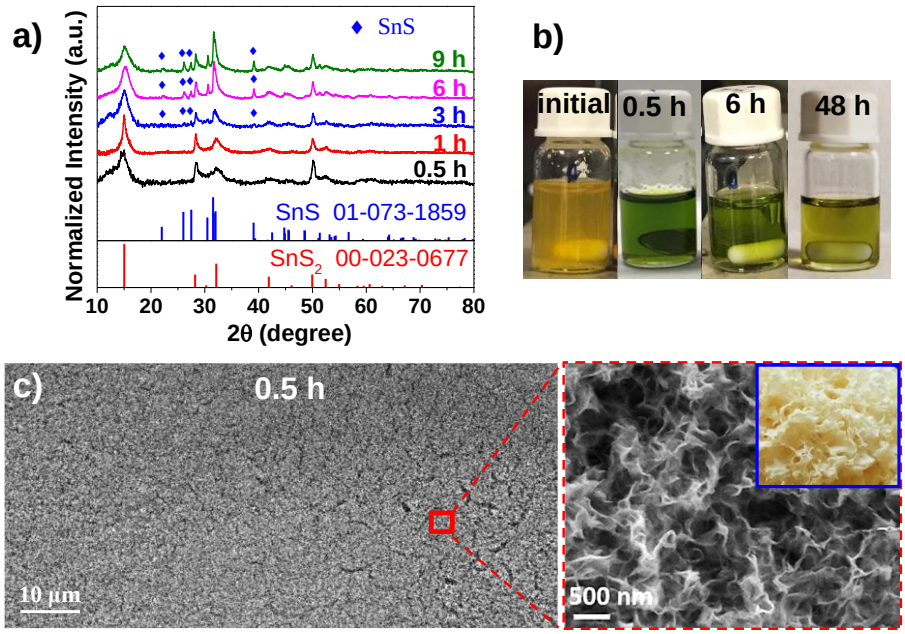

Figure 3. a) XRD patterns of samples recovered after annealing the layers obtained from molecular inks prepared after different dissolution times from 0.5 h to 9 h, as noted; b) Optical photos of respective molecular inks before and after heating at 70 °C for varied range of times. Ink composition and dissolution temperature: Sn/S=1/3, En/Edt=20/1, 70 ºC. c) Large area SEM micrograph and higher magnification image of sample recovered from the annealing of a layer produced from a standard ink: Sn/S=1/3, En/Edt=20/1, 70 ºC, 0.5 h dissolution time. Inset shows optical photograph of the tremella fungus.

Thermogravimetric (TG) analysis of the yellowish gel-like paste collected after drying the conventional ink at 200 ºC (Figure 4a) displayed a two-step mass loss in the temperature range 200-300 ºC. These steps were associated with the ink decomposition and overall accounted for ca. 65 wt% of the initial mass. At temperatures above 500 ºC an additional mass loss, associated with the sulfur evaporation, was observed. Fourier transform infrared spectroscopy (FTIR, Figure 4b) corroborated the loss of organics after annealing the material at 320 ºC for 30 min, as evidenced by the complete loss of strong ν(N-H)/ν(O-H) and ν(C-H) stretching bands originating from the solvent mixture. The absence of bands corresponding to the ν(S-H) thiol group at 2560 cm^{-1} implies that Edt is fully deprotonated by En.[42]

EDX elemental mapping of the films obtained from the deposition and annealing of the conventional ink showed a uniform distribution of S and Sn (Figure S6). High-resolution transmission electron microscopy (HRTEM) micrographs confirmed the SnS_2 hexagonal phase (space group = P63mc) with a=b=3.6450 Å, c=11.8020 Å (Figure 4a, S7). HRTEM analysis reported in Figure 4d shows the overlapping of two 2 different [0001]-oriented nanosheets. The power spectrum (Fast Fourier Transform) applied to the HRTEM image with the applied reciprocal space frequency

(structural) filtering showed the presence of a 21º rotation between the overlapping nanosheets (Figure 4d). These results confirmed the pileup of different nanosheets, consistently with SEM results. UV-vis analysis of recovered SnS_2 films (Figure 4c) showed their bandgap to be around 2.5 eV, which is consistent with the relatively wide range of optical bandgaps reported for SnS_2.[41,45] The small deviation on the experimental band gap values measured here with respect to theoretical SnS_2 values can be ascribed to the reduced thickness of the produced SnS_2 layer (Figure 1f, 3c and 4d), consistently with previous report.[46]

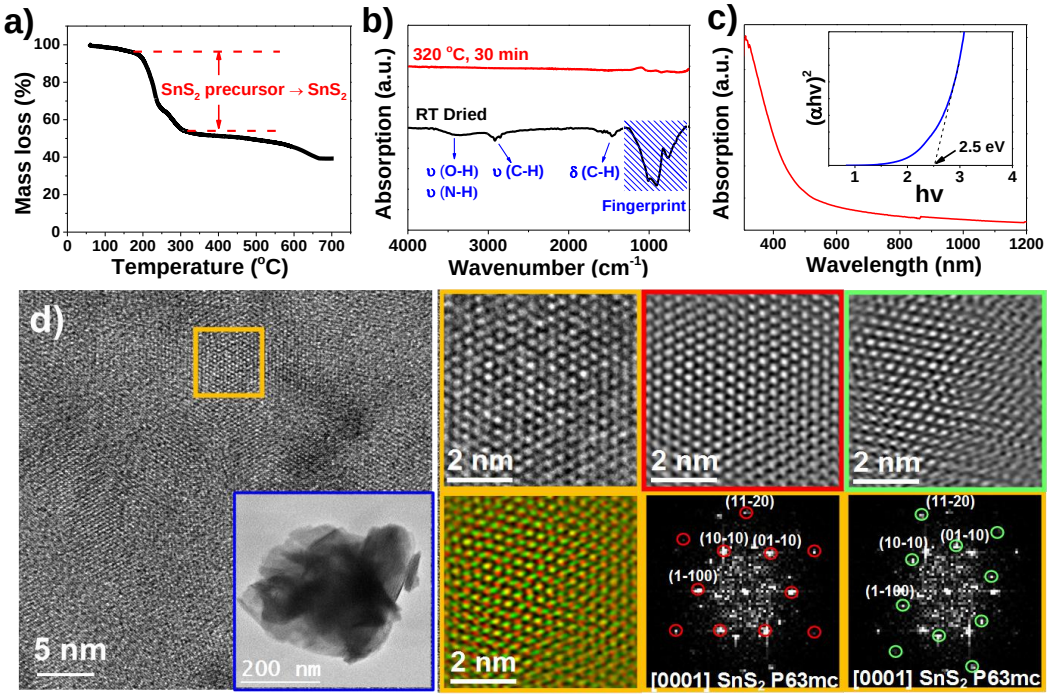

Figure 4. SnS_2 recovered from a conventional molecular ink: a) TG profile of a SnS_2 molecular ink after drying at 200 ºC. b) FTIR spectra of a SnS_2 molecular ink dried at room temperature and of the material recovered after annealing at 320 ºC for 30 min. c) UV-Vis spectrum of the material recovered after annealing at 320 ºC for 30 min. d) HRTEM micrograph of the material recovered after annealing at 320 ºC for 30 min, detail of the orange squared region and its corresponding power spectrum. From the analyzed crystalline domain, the SnS_2 lattice fringe distances were measured to be 0.316 nm, 0.314 nm, 0.310 and 0.181 nm, at 62.65, 123.67 and 94.00º, which could be interpreted as the hexagonal SnS_2 phase, visualized along its [0001] zone axis. Green and yellow squared images correspond to the reciprocal space frequency filtered reconstructed images corresponding to each individual overlapping nanosheet, as extracted from the orange squared region. The spots used in the frequency reconstruction have been circled in red and green, respectively, in the power spectra provided below.

To study the photocatalytic properties of SnS_2 tremella layers obtained from the molecular ink, the ink was deposited on fluorine doped tin oxide (FTO)-coated glass substrates by drop casting. The annealed layer was used as anode in a photoelectrochemical (PEC) cell for water splitting. XRD and SEM analysis confirmed the phase and structure of the SnS_2 to be maintained when depositing the

ink over FTO instead of glass (Figure S8). Using these SnS_2 layers, current densities reaching up to ~160 μA/cm^2 (1.23 V *vs.* RHE) were measured (Figure 5). This performance was well above that of previously reported bare SnS_2 photoanodes,[47] and even better than some SnS_2 samples incorporating co-catalysts (Table S5).[48–52] We ascribed this excellent photocurrents to: 1) the tremella morphology that provided a larger interface area with the electrolyte and effective paths for the solution diffusion; 2) the intimate contact of the SnS_2 absorber with the FTO current collector, thus decreasing the interphase electrical resistance and facilitating the transfer of photogenerated charges from the SnS_2 photocatalyst films to the FTO.

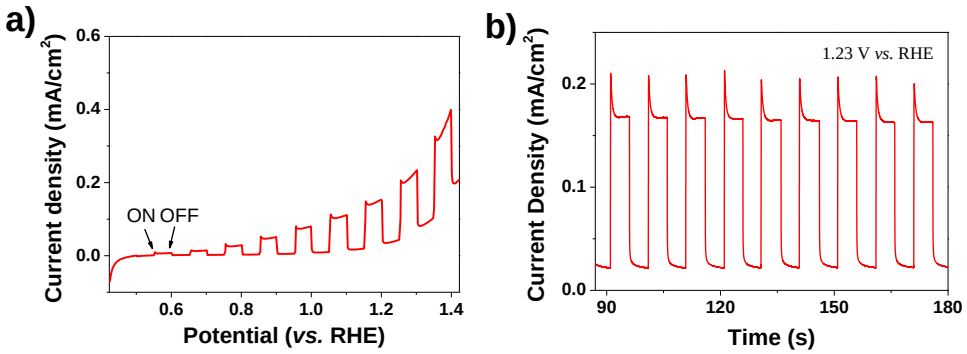

Figure 5. a) Linear sweep voltammogram and b) amperometric i-t curve at 1.23 V vs RHE of a SnS_2/FTO sample under chopped illumination. RHE: reversible hydrogen electrode.

We further investigated the conformal coating of SnS_2 on different substrates. As an example, stainless steel (SS) meshes were coated through a quick immersion of the preheated support on the molecular ink and the posterior drying and annealing of the obtained film (see experimental section for details). Using this simple procedure, homogeneous layers of nanostructured SnS_2 could be coated on the surface of SS meshes as observed by SEM, EDX and SEM mapping (Figures S9 and S10). Notice that since the mixture of En/Edt has a high metal dissolution power, the coating of Ni and Cu foams/meshes using this ink inevitably resulted in Ni or Cu contamination in the final SnS_2 layer. As an alternative, instead of SS, corrosion-free carbon cloth (CC) was used as current collector. Figure S11 displays SEM micrographs of bare and SnS_2-coated CCs.

A different strategy was used to coat graphene flakes. GO produced by the Hummers method was introduced in the precursor solution. During the ink formulation, simultaneously to the dissolution of Sn and S powders, GO was reduced by the amine,[53,54] yielding an ink containing a mixture of Sn-S molecular precursor and rGO. This composite inkcould be used to coat virtually any substrate with SnS_2/rGO composite layers using the above coating and annealing steps (Figure S12).

We used the same strategy to produce $SnS_{2-x}Se_x$ coatings with controlled S/Se ratios, by simply adding the proper amount of Se in the precursor solution (see experimental section for details). As can be seen in Figure 6a, an obvious XRD peak shift towards lower angle occurred when Se ratio increased from 0 to 100 %, indicating the Se ion entered within the crystal structure. No impurity peaks were detected, even when pure $SnSe_2$ was recovered. The phase purity obtained in the present work was in contrast with results obtained by McCarthy et al., who systematically obtained sulfide impurities when attempting to produce pure $CoSe_2$.[55] Differences are associated with the very little amount of Edt used in the present work. Figure S13 shows how the color of the precursor solution changed from green to dark brown with the selenium dosage increase. Figure 6b displays how the color of spin-coated thin-film changed after annealing. SEM-EDX data (Table S4) demonstrated the sum of Se and S to be always around 67 %, while the tin composition was around 33 %, confirming that Se ions occupied the position of S within $SnS_{2-x}Se_x$ ternary chalcogenides. SEM analysis further showed the tremella-like morphology to change into sheet-like with the addition of Se (Figure 6c). Additionally, the band gap energy decreased from 2.50 eV (SnS_2) to 1.65 eV ($SnSe_2$) with Se incorporation (Figure 6d).

$SnS_{2-x}Se_x$/FTO electrodes displayed a negative photoconductivity at -0.1 V (or lower) *vs.* Ag/AgCl. Among the samples containing Se, the highest photocurrents were measured from $SnSe_2$/FTO photoelectrodes, reaching up to 10 $\mu A/cm^2$ at -0.1 V *vs.* Ag/AgCl (Figure S14).

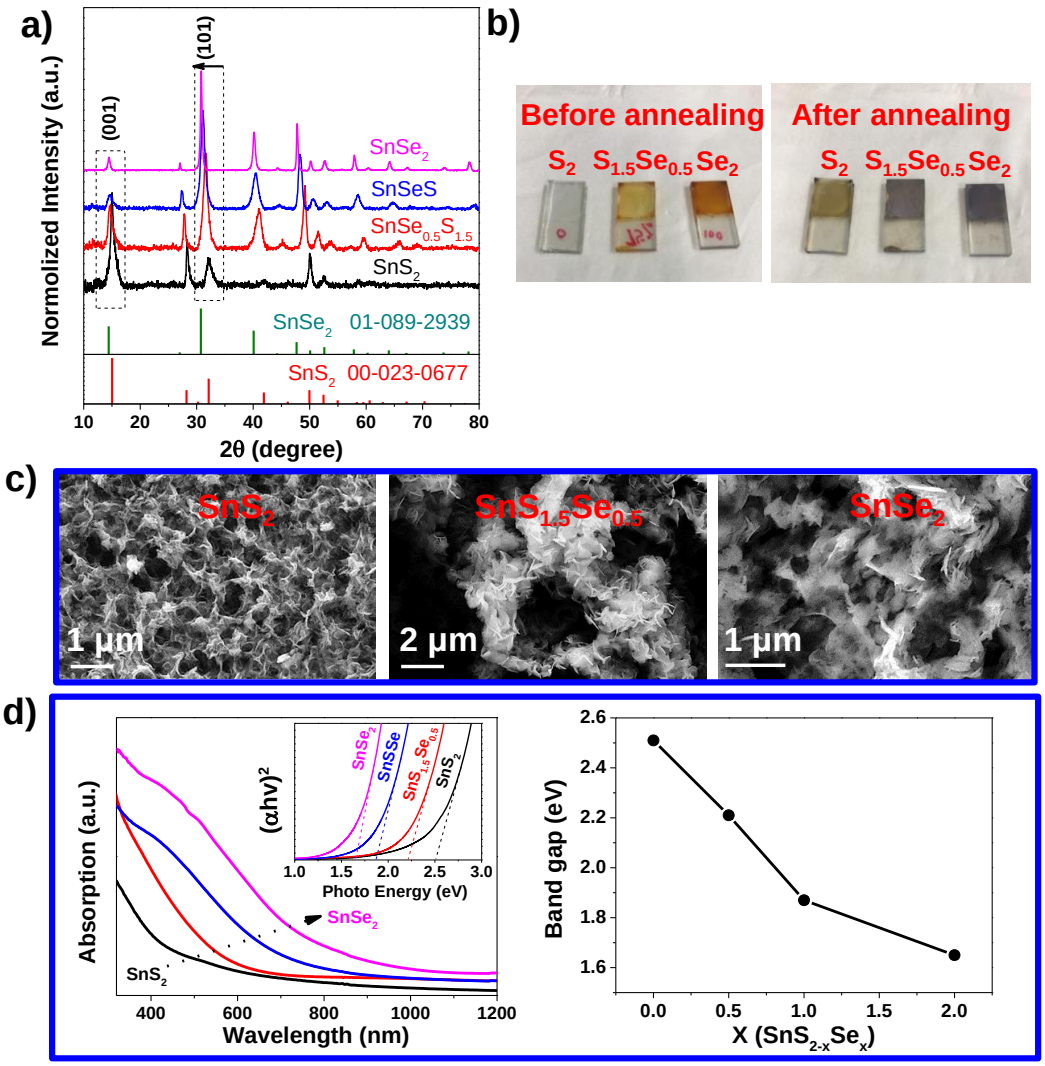

Figure 6. $SnS_{2-x}Se_x$ ternary chalcogenides obtained from the annealing for layers produced from inks containing different S/Se ratios: a) XRD patterns; b) optical photograph of $SnS_{2-x}Se_x$/FTO layers before and after annealing; c) SEM micrographs; d) UV-Vis spectra.

We additionally studied the potential of this precursor ink to produce gram scale amounts of unsupported particles, which can be potentially used in catalysis [36], batteries,[8] photodetectors,[56] sensors,[57] field-effect transistor devices,[58] etc. With this aim, large amounts of SnS_2 molecular ink (5 mL) were decomposed inside a heated flask (see experimental section and Figure S15a for details). After annealing, a gray powder was collected, which turned gray-yellow after washing. XRD analysis showed the powder to be phase pure SnS_2 (Figure S15b). X-ray photoelectron spectroscopy (XPS) analysis showed the Sn 3d region to display a unique doublet at 495.9 eV (Sn $3d_{3/2}$) and 487.5 eV (Sn $3d_{5/2}$), associated with Sn^{4+} within the SnS_2 lattice, [59-61] while the S 2p region showed a doublet at 163.5 eV (S $2p_{1/2}$) and 162.3 eV (S $2p_{3/2}$), ascribed to S^{2-} in the SnS_2 lattice [60,61] (Figure 7a). Besides, SEM-EDX data in Figure 7b further confirmed that the composition of Sn/S was ca. 1/2, consistent

with stoichiometric SnS_2. Interestingly, the powder displayed a flake-like morphology in contrast to the tremella-like particles recovered on substrates, which was ascribed to the additional growth of the crystals recovered in powder form associated with the larger amount of available precursor.

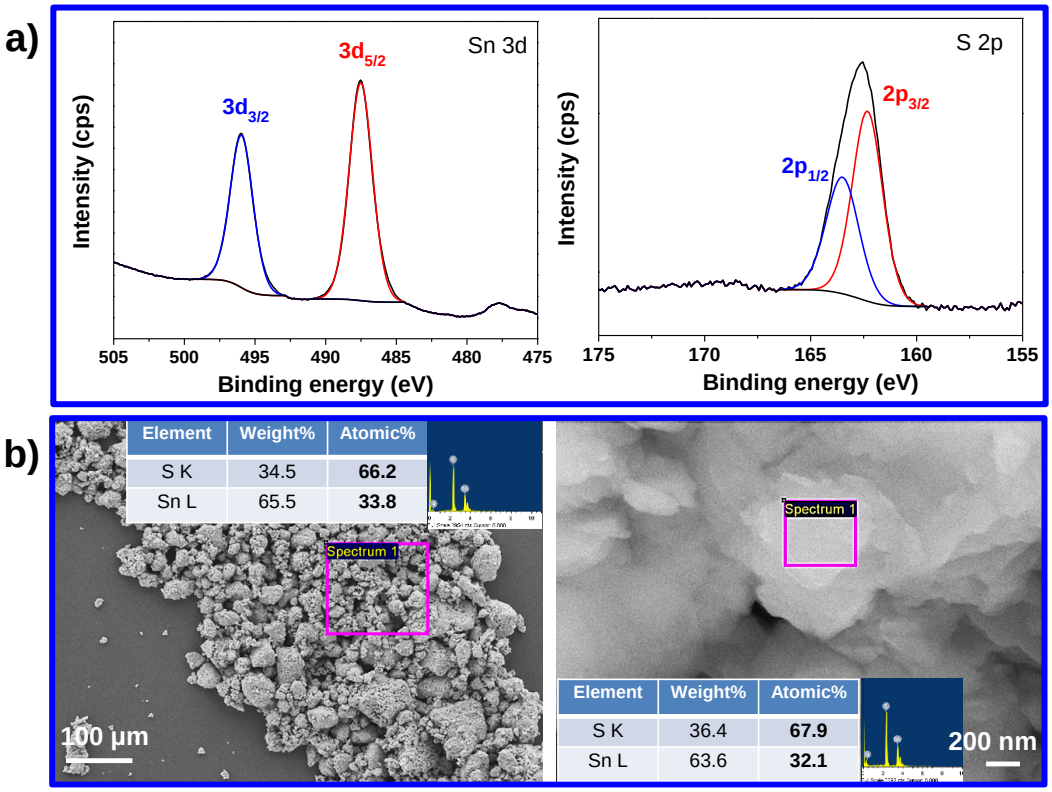

Figure 7. SnS_2 powder recovered from the annealing of large amounts of molecular ink: a) XPS spectra of Sn 3d region and S 2p regions. b) SEM micrographs and EDX data.

CONCLUSIONS

In summary, a Sn-S molecular ink was produced by dissolving Sn and S elemental powders in an amine/thiol co-solvent. The decomposition and annealing of this ink at 320 ºC for 30 min resulted in the formation of nanostructured tin sulfide. Pure SnS_2 layers with a tremella morphology were obtained using an ink containing an elemental ratio Sn/S=1/3 and a solvent ratio En/Edt=20/1. A loss of sulfur in the form of H_2S gas during dissolution was identified as the reason behind the presence of SnS impurities in inks produced using too long dissolution times. This molecular ink could be applied to produce planar and conformal SnS_2 nanostructured layer on conductive substrates, such as FTO, SS and CC. SnS_2/FTO photoanodes provided outstanding photocurrent densities under illumination with simulated solar light. Besides, SnS_2/rGO composites and $SnS_{2-x}Se_x$ were easily

synthesized using the same strategy by simply introducing GO and Se powder in the initial precursor solution.

EXPERIMENTAL SECTION

Chemicals. All chemicals were used as received, without additional purification. Sn powder (99+ %), S powder (99.98 %), En (99.5+ %), Edt (98+ %) were purchased from Sigma-Aldrich. Se powder (99.5+ %) was purchased from Acros Organics. All chemical manipulation and material preparation processes were carried out in an argon-filled glove box.

Ink Preparation. Tin and sulfur elemental powders, other than their salts, were selected as solutes to avoid any potential counterion contamination. To prepare a Sn-S molecular ink, elemental Sn (0.5 mmol) and S (1.5 mmol) powders were weighted and transferred into a glass vial (4 mL). En (2 mL) and Edt (0.1 mL) were sequentially added into the vial. The mixture was then stirred at 750 rpm and heated to 70 °C and kept at this temperature for 30 min to get an optical transparent green ink solution. To study the influence of ratio between En and Edt, different amount of Edt was used, while En amount kept unchanged. To study the influence of sulfur amount, we used different amount of sulfur.

Recovery of Semiconductor Film on Planar Glass Slides. Typically, 0.1 mL of molecular ink was drop casted on a microscope glass slide (~1×1 cm), and then the deposited substrate was heated on a hot plate (Corning, PC400D) at 200 °C to dry the ink. The dried precursor film was afterward annealed at 320 °C on the hotplate for 30 min. These operations were conducted in the argon-filled glovebox. The obtained film was scraped off of the substrate for posterior characterization by XRD, SEM and HRTEM.

Recovery of Semiconductor Film on FTO-coated Glass Slides. 20 μL of molecular ink was drop casted on the surface of FTO with an active area of 1cm×1cm (an additional area of 1cm×1cm was covered by the high-temperature bearable tape to leave a clean area for electrical connection). The tip of the pipette-pipe was used to pull the solution in order to produce a uniform coverage (in this operation, the tip shouldn't touch the FTO surface), after then dried at 200 °C and finally annealed on the hot plate at 320 °C for 30 min.

Recovery of Semiconductor Film on Stainless Steel and Carbon Cloth. Typically, a piece of pre-cleaned SS was firstly heated on the hot plate at 200 °C for several minutes, then quickly immerse into molecular ink and hold for 30 s. The wet SS was then held by a tweezer and put close to the surface of the hot plate to dry, after then annealed in Ar filled tubular furnace at 320 °C for 30 min with a temperature ramp of 3 °C/min. SS was preheated to decrease the local viscosity of the molecular ink close to the SS surface, and thus facilitate it diffusion through the porous electrode

structure. The heated support also promoted the film drying and facilitated the formation of more uniform coatings.

To coat CC with a SnS_2 layer, 40 μL of molecular ink was evenly drop casted on two sides of a 1x1 cm^2 carbon cloth using the tip of the pipette to spread the precursor solution and then put close to the surface of the hot plate to dry, subsequently annealed in Ar filled tubular furnace at 320 °C for 30 min with a temperature ramp of 3 °C/min.

Recovery of SnS_2/rGO Composites. GO was produced by the Hummers method as originally presented by Kovtyukhova.[62] In the next step, 10 mg of GO was added together with Sn powder and S powder to formulate the Sn-S molecular ink. The same ratios of Sn/S and En/Edt and dissolution and annealing times and temperatures as used in conventional inks were used to recover SnS_2/rGO composite layers.

Recovery of $SnS_{2-x}Se_x$. A proper amount of elemental Se powder was introduced in the initial mixture in replacement of the same molar amount of S powder. The dissolution time was adjusted to make sure that all the precursor powders were dissolved and an optical transparent molecular solution was obtained. Dissolution time was typically 30 min for SnS_2 and increased up to 80 min with Se amount increasing. Dissolution temperature was set at 70 ºC in all cases. The same drying and annealing steps used to recover pure-phase SnS_2 were used to recover $SnS_{2-x}Se_x$, except that the annealing time was increase to 60 min.

To coat $SnS_{2-x}Se_x$ on FTO for posterior PEC measurements, we noticed that the recovered $SnS_{2-x}Se_x$, especially $SnSe_2$, using the same spin coating method as we did on SnS_2/FTO showed almost no i-t response. We attributed this result to the $SnSe_2$ layer being too thick. Notice $SnSe_2$ has a much lower band gap and thus absorbs light much more strongly, thus thinner layers are required. Too thick layers prevent light from arriving to the semiconductor-electrode interphase and decrease performance. We thus used the spin coating method to produce thinner layers, and kept all the deposition process the same to make the results comparable.

Recovery of Large-scaled Powder. 5 mL of Sn-S molecular ink was injected into a 50 mL three-neck flask preheated 300 °C and containing an Ar atmosphere. A safety flask containing water/ethanol was used to collect the gas/vapor emanated from the ink solution. Upon ink injection, temperature decreased to ~200 °C and then increased slowly to 300 °C. The flask was kept at this temperature for additional 10 min to obtain a dry powder. The powder was then grinded and annealed in tubular furnace under Ar atmosphere at 350 °C for 2 hours with a ramp rate of 3 °C/min or lower. The annealed powder was washed using CS_2 and ethanol by sonication to remove the potential sulfur

residues. The sample was finally dried for posterior characterizations and use. It should be noted that we injected the precursor solution very fast in order to make the heating process more uniform and synthesis more repeatable, and thus minimizing the difference among different batches.

Sample Characterization. XRD patterns were obtained on a Bruker AXS D8 ADVANCE X-ray diffractometer (Bruker, Karlsruhe, Germany) operating at 40 kV and 40 mA with Ni-filtered (2 μm thickness) Cu Kα1 radiation (λ = 1.5406 Å). TEM characterization was carried out on a ZEISS LIBRA 120 (Carl Zeiss, Jena, Germany), operating at 120 kV. HRTEM images were obtained using a field emission gun FEI Tecnai F20 microscope at 200 kV with a point-to-point resolution of 0.19 nm. For TEM characterization, samples were prepared by peeling off directly from glass slide and drop casting their ethanol solutions onto a 200 mesh copper grid. SEM analysis was done in a ZEISS Auriga microscope (Carl Zeiss, Jena, Germany) with an EDX detector at 20 kV to study composition. XPS was carried out on a SPECS system (SPECS GmbH, Berlin, Germany) equipped with an Al anode XR50 source operating at 150 W and a Phoibos 150 MCD-9 detector (SPECS GmbH, Berlin, Germany). The pressure in the analysis chamber was kept below 10^{-7} Pa. Data processing was performed with the CasaXPS program (Casa Software Ltd., UK). Binding energy (BE) values were centered by using the C 1s peak at 284.8 eV. TG analysis was carried out using a PerkinElmer Diamond TG/DTA instrument (PerkinElmer, Walthham, MA, USA). For TG analysis, a proper amount of molecular ink was dried on a glass slide at 200 °C and scratched out after cooling down and ~20 mg of the dried gel powder was collected and loaded into a ceramic pan. Measurements were carried out in an Ar atmosphere from room temperature to 700 °C at a heating rate of 5 °C/min. FTIR was performed on an Alpha Bruker FTIR spectrometer with a platinum attenuated total reflectance (ATR) single reflection module. FTIR data were typically averaged over 24 scans. UV-vis absorption spectra were acquired with a PerkinElmer LAMBDA 950 UV-vis spectrophotometer equipped with an integrating sphere. For FTIR and UV-vis analysis, films were produced by spin coating on glass substrates instead of drop-casting.

Photoelectrochemical Measurements. PEC characterization was performed in a three-electrode system using an electrochemical workstation (Metrohm Autolab). A Pt mesh (2 cm^2 surface area) and Ag/AgCl (3.3 M KCl) were used as the counter and reference electrodes, respectively. $SnS_{2-x}Se_x$ films deposited on FTO were used as working electrode. Before film deposition, the FTO glass was washed with acetone-isopropanol (1-1 volume), ethanol, and then deionized water. An aqueous solution of Na_2SO_4 (0.5 M, pH = 7) was used as the electrolyte. Relatively thick SnS_2 films deposited by drop casting were used to test the SnS_2 PEC performance. On the other hand, thinner films produced by spin coating were used to the $SnSe_2$ performance owing to the higher light absorption capability of

this material associated to its lower band gap. The electrolyte was purged with Ar for 30 min prior to the measurement. The incident light source was provided by 8 radially distributed 35 W xenon lamps, providing a total irradiance power on the sample of ca. 100 mW/cm^2. The following formula was used to convert the potentials to the RHE standard scale:

$$E \textit{ vs. } RHE = E_{Ag/AgCl} + E^{o}_{Ag/AgCl} + 0.059 \times pH = E_{Ag/AgCl} + 0.623 \text{ (V)}$$

ASSOCIATED CONTENT

Supporting Information

The Supporting Information is available free of charge on the ACS Publications website at DOI: *******.

Electronic supplementary information (ESI) available: Additional experiments, SEM, XRD, EDX, TEM, PEC tests, scheme of large-scale procedure and Tables of composition change evolution and PEC performance comparison.

AUTHOR INFORMATION

Corresponding Author

*Email: acabot@irec.cat

Notes

The authors declare no competing financial interest.

ACKNOWLEDGEMENTS

This work was supported by the European Regional Development Funds and by the Spanish Ministerio de Economía y Competitividad through the project SEHTOP, ENE2016-77798-C4-3-R, and ENE2017-85087-C3. Y.Z. thanks the China Scholarship Council for the scholarship support (No. 201606500001). Authors acknowledge funding from Generalitat de Catalunya 2017 SGR 327 and 2017 SGR 1246. ICN2 acknowledges support from the Severo Ochoa Programme (MINECO, Grant no. SEV-2017-0706) and is funded by the CERCA Programme/Generalitat de Catalunya. J. Llorca is a Serra Húnter Fellow and is grateful to ICREA Academia program and to MINECO/FEDER grant

RTI2018-093996-B-C31 and GC 2017 SGR 128. Part of the present work has been performed in the framework of Universitat Autònoma de Barcelona Materials Science PhD program. T.Z. has received funding from the CSC-UAB PhD scholarship program.

REFERENCES

(1) McCarthy, C. L.; Webber, D. H.; Schueller, E. C.; Brutchey, R. L. Solution-Phase Conversion of Bulk Metal Oxides to Metal Chalcogenides Using a Simple Thiol-Amine Solvent Mixture. *Angew. Chemie - Int. Ed.* **2015**, *54*, 8378–8381.

(2) Vayssieres, L.; Beermann, N.; Lindquist, S. E.; Hagfeldt, A. Controlled Aqueous Chemical Growth of Oriented Three-Dimensional Crystalline Nanorod Arrays: Application to Iron(III) Oxides. *Chem. Mater.* **2001**, *13*, 233–235.

(3) McCarthy, C. L.; Brutchey, R. L. Preparation of Electrocatalysts Using a Thiol-Amine Solution Processing Method. *Dalton Transactions*. **2018**, 5137–5143.

(4) Mitzi, D. B. *Solution Processing of Inorganic Materials*; John Wiley & Sons: Hoboken, NJ, 2009.

(5) Li, J.; Luo, Z.; Zuo, Y.; Liu, J.; Zhang, T.; Tang, P.; Arbiol, J.; Llorca, J.; Cabot, A. NiSn Bimetallic Nanoparticles as Stable Electrocatalysts for Methanol Oxidation Reaction. *Appl. Catal. B Environ.* **2018**, *234*, 10–18.

(6) Li, J.; Zuo, Y.; Liu, J.; Wang, X.; Yu, X.; Du, R.; Zhang, T.; Infante-Carrió, M. F.; Tang, P.; Arbiol, J.; Llorca, J.; Luo, Z.; Cabot, A. Superior methanol electrooxidation performance of (110)-faceted nickel polyhedral nanocrystals. *J. Mater. Chem. A* **2019**, *7*, 22036-22043.

(7) Li, Y.; Meng, J.; Yu, Z.; Li, Y. PdS-Modified CdS/NiS Composite as an Efficient Photocatalyst for H_2 evolution in Visible Light. *Catal. Today* **2014**, *225*, 136–141.

(8) Liu, Y.; Kang, H.; Jiao, L.; Chen, C.; Cao, K.; Wang, Y.; Yuan, H. Exfoliated-SnS_2 Restacked on Graphene as a High-Capacity, High-Rate, and Long-Cycle Life Anode for Sodium Ion Batteries. *Nanoscale* **2015**, *7*, 1325–1332.

(9) Zuo, Y.; Ni, J.; Song, J.; Niu, H.; Mao, C.; Zhang, S.; Shen, Y. Synthesis of Co_3O_4/NiO nanofilms and their enhanced electrochemical performance for supercapacitor application. *Appl. Surf. Sci.* **2016**, *370*, 528-535.

(10) Li, J.; Luo, Z.; He, F.; Zuo, Y.; Zhang, C.; Liu, J.; Yu, X.; Du, R.; Zhang, T.; Infante-Carrió, M. F.; Tang, P.; Arbiol, J.; Llorca, J.; Cabot, A. Colloidal Ni-Co-Sn nanoparticles as efficient electrocatalysts for the methanol oxidation reaction. *J. Mater. Chem. A* **2018**, *6*, 22915-22924.

(11) Chlistunoff, J.; Sansiñena, J. M. On the Use of Nafion® in Electrochemical Studies of Carbon Supported Oxygen Reduction Catalysts in Aqueous Media. *J. Electroanal. Chem.* **2016**, *780*, 134–146.

(12) Mitzi, D. B.; Kosbar, L. L.; Murray, C. E.; Copel, M.; Afzali, A. High-Mobility Ultrathin Semiconducting Films Prepared by Spin Coating. *Nature* **2004**, *428*, 299–303.

(13) Mitzi, D. B. Synthesis, Structure, and Thermal Properties of Soluble Hydrazinium

Germanium(IV) and Tin(IV) Selenide Salts. *Inorg. Chem.* **2005**, *44*, 3755–3765.

(14) Mitzi, D. B. $N_4H_9Cu_7S_4$: A Hydrazinium-Based Salt with a Layered Cu_7S_4- Framework. *Inorg. Chem.* **2007**, *46*, 926–931.

(15) Mitzi, D. B.; Copel, M.; Chey, S. J. Low-Voltage Transistor Employing a High-Mobility Spin-Coated Chalcogenide Semiconductor. *Adv. Mater.* **2005**, *17*, 1285–1289.

(16) Mitzi, D. B. Polymorphic One-Dimensional $(N_2H_4)_2ZnTe$: Soluble Precursors for the Formation of Hexagonal or Cubic Zinc Telluride. *Inorg. Chem.* **2005**, *44*, 7078–7086.

(17) Mitzi, D. B.; Copel, M.; Murray, C. E. High-Mobility p-Type Transistor Based on a Spin-Coated Metal Telluride Semiconductor. *Adv. Mater.* **2006**, *18*, 2448–2452.

(18) Milliron, D. J.; Raoux, S.; Shelby, R. M.; Jordan-Sweet, J. Solution-Phase Deposition and Nanopatterning of GeSbSe Phase-Change Materials. *Nat. Mater.* **2007**, *6*, 352–356.

(19) Milliron, D. J.; Mitzi, D. B.; Copel, M.; Murray, C. E. Solution-Processed Metal Chalcogenide Films for p-Type Transistors. *Chem. Mater.* **2006**, *18*, 581–590.

(20) McCarthy, C. L.; Brutchey, R. L. Solution Processing of Chalcogenide Materials Using Thiol-Amine "Alkahest" Solvent Systems. *Chem. Commun.* **2017**, *53*, 4888–4902.

(21) Webber, D. H.; Brutchey, R. L. Alkahest for V_2VI_3 Chalcogenides: Dissolution of Nine Bulk Semiconductors in a Diamine-Dithiol Solvent Mixture. *J. Am. Chem. Soc.* **2013**, *135*, 15722–15725.

(22) Vineyard, B. D. Versatility and the Mechanism of the N-Butyl-Amine-Catalyzed Reaction of Thiols with Sulfur. *J. Org. Chem.* **1967**, *32*, 3833–3836.

(23) Lin, Z.; He, Q.; Yin, A.; Xu, Y.; Wang, C.; Ding, M.; Cheng, H. C.; Papandrea, B.; Huang, Y.; Duan, X. Cosolvent Approach for Solution-Processable Electronic Thin Films. *ACS Nano* **2015**, *9*, 4398–4405.

(24) Zhao, X.; Zhang, R.; Handwerker, C.; Agrawal, R. The Potential of Amine-Thiol Based Solution Processing for Chalcogenide Photovoltaics. In *2016 IEEE 43rd Photovoltaic Specialists Conference (PVSC)*; IEEE, **2016**, 0542–0544.

(25) Agrawal, R.; Zhang, R.; Walker, B. C.; Handwerker, C. Homogeneous Precursor Formation Method and Device Thereof. US 9738799 B2, August 12, 2015.

(26) Zhang, R.; Cho, S.; Lim, D. G.; Hu, X.; Stach, E. A.; Handwerker, C. A.; Agrawal, R. Metal–Metal Chalcogenide Molecular Precursors to Binary, Ternary, and Quaternary Metal Chalcogenide Thin Films for Electronic Devices. *Chem. Commun.* **2016**, *52*, 5007–5010.

(27) McCarthy, C. L.; Brutchey, R. L. Solution Processing of Chalcogenide Materials Using Thiol-Amine "Alkahest" Solvent Systems. *Chem. Commun.* **2017**, *53*, 4888–4902.

(28) Lei, Y. M.; Zhou, J.; Chai, Y. Q.; Zhuo, Y.; Yuan, R. SnS_2 Quantum Dots as New Emitters with Strong Electrochemiluminescence for Ultrasensitive Antibody Detection. *Anal. Chem.* **2018**, *90*, 12270–12277.

(29) Giri, B.; Masroor, M.; Yan, T.; Kushnir, K.; Carl, A. D.; Doiron, C.; Zhang, H.; Zhao, Y.; McClelland, A.; Tompsett, G. A.; Wang, D. W.; Grimm, R. L.; Titova, L. V.; Rao, P. M.

Balancing Light Absorption and Charge Transport in Vertical SnS_2 Nanoflake Photoanodes with Stepped Layers and Large Intrinsic Mobility. *Adv. Energy Mater.* **2019**, *9*, 1901236.

(30) Meng, L.; Wang, S.; Cao, F.; Tian, W.; Long, R.; Li, L. Doping-Induced Amorphization, Vacancy, and Gradient Energy Band in SnS_2 Nanosheet Arrays for Improved Photoelectrochemical Water Splitting. *Angew. Chemie - Int. Ed.* **2019**, *58*, 6761–6765.

(31) Du, Y.; Yin, Z.; Rui, X.; Zeng, Z.; Wu, X. J.; Liu, J.; Zhu, Y.; Zhu, J.; Huang, X.; Yan, Q.; Zhang, H. A Facile, Relative Green, and Inexpensive Synthetic Approach toward Large-Scale Production of SnS_2 nanoplates for High-Performance Lithium-Ion Batteries. *Nanoscale* **2013**, *5*, 1456–1459.

(32) Zhang, Y.; Lu, J.; Shen, S.; Xu, H.; Wang, Q. Ultralarge Single Crystal SnS Rectangular Nanosheets. *Chem. Commun.* **2011**, *47* , 5226–5228.

(33) Yin, D.; Liu, Y.; Dun, C.; Carroll, D. L.; Swihart, M. T. Controllable Colloidal Synthesis of Anisotropic Tin Dichalcogenide Nanocrystals for Thin Film Thermoelectrics. *Nanoscale* **2018**, *10*, 2533–2541.

(34) Chakrabarti, A.; Lu, J.; McNamara, A. M.; Kuta, L. M.; Stanley, S. M.; Xiao, Z.; Maguire, J. A.; Hosmane, N. S. Tin(IV) Sulfide: Novel Nanocrystalline Morphologies. *Inorganica Chim. Acta* **2011**, *374*, 627–631.

(35) Zhang, Y. C.; Du, Z. N.; Li, S. Y.; Zhang, M. Novel Synthesis and High Visible Light Photocatalytic Activity of SnS_2 Nanoflakes from $SnCl_2{\cdot}2H_2O$ and S Powders. *Appl. Catal. B Environ.* **2010**, *95*, 153–159.

(36) Sun, Y.; Cheng, H.; Gao, S.; Sun, Z.; Liu, Q.; Liu, Q.; Lei, F.; Yao, T.; He, J.; Wei, S.; Xie, Y. Freestanding Tin Disulfide Single-Layers Realizing Efficient Visible-Light Water Splitting. *Angew. Chemie Int. Ed.* **2012**, *51*, 8727–8731.

(37) Chen, H.; Chen, Y.; Zhang, H.; Zhang, D. W.; Zhou, P.; Huang, J. Suspended SnS_2 Layers by Light Assistance for Ultrasensitive Ammonia Detection at Room Temperature. *Adv. Funct. Mater.* **2018**, *28*, 1801035.

(38) Ying, H.; Li, X.; Wu, Y.; Yao, Y.; Xi, J.; Su, W.; Jin, C.; Xu, M.; He, Z.; Zhang, Q. High-Performance Ultra-Violet Phototransistors Based on CVT-Grown High Quality SnS_2 Flakes. *Nanoscale Adv.* **2019**, *1*, 3973–3979.

(39) Shao, G.; Xue, X. X.; Zhou, X.; Xu, J.; Jin, Y.; Qi, S.; Liu, N.; Duan, H.; Wang, S.; Li, S.; Ouzounian, M; Hu, T. S.; Luo, J; Liu, S; Feng, Y. Shape-Engineered Synthesis of Atomically Thin 1T-SnS_2 Catalyzed by Potassium Halides. *ACS Nano* **2019**, *13*, 8265–8274.

(40) Xu, L.; Zhang, P.; Jiang, H.; Wang, X.; Chen, F.; Hu, Z.; Gong, Y.; Shang, L.; Zhang, J.; Jiang, K.; Chu, J. H. Large-Scale Growth and Field-Effect Transistors Electrical Engineering of Atomic-Layer SnS_2. *Small* **2019**, *15*, 1904116.

(41) Mattinen, M.; King, P. J.; Khriachtchev, L.; Meinander, K.; Gibbon, J. T.; Dhanak, V. R.; Räisänen, J.; Ritala, M.; Leskelä, M. Low-Temperature Wafer-Scale Deposition of Continuous 2D SnS_2 Films. *Small* **2018**, *14*, 1800547.

(42) Buckley, J. J.; McCarthy, C. L.; Del Pilar-Albaladejo, J.; Rasul, G.; Brutchey, R. L. Dissolution of Sn, SnO, and SnS in a Thiol-Amine Solvent Mixture: Insights into the Identity of the Molecular Solutes for Solution-Processed SnS. *Inorg. Chem.* **2016**, *55*, 3175–3180.

(43) Thomson, J. W.; Nagashima, K.; Macdonald, P. M.; Ozin, G. A. From Sulfur−Amine Solutions to Metal Sulfide Nanocrystals: Peering into the Oleylamine-Sulfur Black Box. *J. Am. Chem. Soc.* **2011**, *133*, 5036–5041.

(44) Kim, E. T.; Chung, W. J.; Lim, J.; Johe, P.; Glass, R. S.; Pyun, J.; Char, K. One-Pot Synthesis of PbS NP/Sulfur-Oleylamine Copolymer Nanocomposites via the Copolymerization of Elemental Sulfur with Oleylamine. *Polym. Chem.* **2014**, *5*, 3617–3623.

(45) Ye, G.; Gong, Y.; Lei, S.; He, Y.; Li, B.; Zhang, X.; Jin, Z.; Dong, L.; Lou, J.; Vajtai, R.; Zhou, W.; Ajayan, P. M. Synthesis of Large-Scale Atomic-Layer SnS_2 through Chemical Vapor Deposition. *Nano Res.* **2017**, *10*, 2386–2394.

(46) Mukhokosi, E. P.; Krupanidhi, S. B.; Nanda, K. K. Band Gap Engineering of Hexagonal $SnSe_2$ Nanostructured Thin Films for InfraRed Photodetection. *Sci. Rep.* **2017**, *7*, 15215.

(47) Yu, J.; Xu, C. Y.; Ma, F. X.; Hu, S. P.; Zhang, Y. W.; Zhen, L. Monodisperse SnS_2 Nanosheets for High-Performance Photocatalytic Hydrogen Generation. *ACS Appl. Mater. Interfaces* **2014**, *6*, 22370–22377.

(48) Liu, Y.; Chen, P.; Chen, Y.; Lu, H.; Wang, J.; Yang, Z.; Lu, Z.; Li, M.; Fang, L. In Situ Ion-Exchange Synthesis of SnS_2/g-C_3N_4 Nanosheets Heterojunction for Enhancing Photocatalytic Activity. *RSC Adv.* **2016**, *6*, 10802–10809.

(49) Meng, H.; Wang, T.; Yu, X.; Zhu, Y.; Zhang, Y. BiOCl/SnS_2 hollow Spheres for the Photocatalytic Degradation of Waste Water. *RSC Adv.* **2015**, *5*, 107088–107097.

(50) Liu, Y.; Geng, P.; Wang, J.; Yang, Z.; Lu, H.; Hai, J.; Lu, Z.; Fan, D.; Li, M. In-Situ Ion-Exchange Synthesis Ag_2S Modified SnS_2 nanosheets toward Highly Photocurrent Response and Photocatalytic Activity. *J. Colloid Interface Sci.* **2018**, *512*, 784–791.

(51) Wang, L.; Jin, G.; Shi, Y.; Zhang, H.; Xie, H.; Yang, B.; Sun, H. Co-Catalyst-Free ZnS-SnS_2 porous Nanosheets for Clean and Recyclable Photocatalytic H_2 generation. *J. Alloys Compd.* **2018**, *753*, 60–67.

(52) Zuo, Y.; Liu, Y.; Li, J.; Du, R.; Yu, X.; Xing, C.; Zhang, T.; Yao, L.; Arbiol, J.; Llorca, J.; Sivula, K.; Guijarro, N.; Cabot; A. Solution-Processed Ultrathin SnS_2-Pt Nanoplates for Photoelectrochemical Water Oxidation. *ACS Appl. Mater. Interfaces* **2019**, *11*, 6918–6926.

(53) Huang, H. H.; De Silva, K. K. H.; Kumara, G. R. A.; Yoshimura, M. Structural Evolution of Hydrothermally Derived Reduced Graphene Oxide. *Sci. Rep.* **2018**, *8* , 6849.

(54) Li, X.; Hao, Z.; Zhang, F.; Li, H. Reduced Graphene Oxide-Immobilized Tris(Bipyridine)Ruthenium(II) Complex for Efficient Visible-Light-Driven Reductive Dehalogenation Reaction. *ACS Appl. Mater. Interfaces* **2016**, *8*, 12141–12148.

(55) McCarthy, C. L.; Downes, C. A.; Schueller, E. C.; Abuyen, K.; Brutchey, R. L. Method for the Solution Deposition of Phase-Pure $CoSe_2$ as an Efficient Hydrogen Evolution Reaction Electrocatalyst. *ACS Energy Lett.* **2016**, *1*, 607–611.

(56) Fu, X.; Ilanchezhiyan, P.; Mohan Kumar, G.; Cho, H. D.; Zhang, L.; Chan, A. S.; Lee, D. J.; Panin, G. N.; Kang, T. W. Tunable UV-Visible Absorption of SnS_2 Layered Quantum Dots Produced by Liquid Phase Exfoliation. *Nanoscale* **2017**, *9*, 1820–1826.

(57) Lee, K. T.; Liang, Y. C.; Lin, H. H.; Li, C. H.; Lu, S. Y. Exfoliated SnS_2 Nanoplates for

Enhancing Direct Electrochemical Glucose Sensing. *Electrochim. Acta* **2016**, *219*, 241–250.

(58) Huang, Y.; Sutter, E.; Sadowski, J. T.; Cotlet, M.; Monti, O. L. A.; Racke, D. A.; Neupane, M. R.; Wickramaratne, D.; Lake, R. K.; Parkinson, B. A.; Sutter, P. Tin Disulfide-an Emerging Layered Metal Dichalcogenide Semiconductor: Materials Properties and Device Characteristics. *ACS Nano* **2014**, *8*, 10743–10755.

(59) Jiang, Y.; Wei, M.; Feng, J.; Ma, Y.; Xiong, S. Enhancing the Cycling Stability of Na-Ion Batteries by Bonding SnS_2 Ultrafine Nanocrystals on Amino-Functionalized Graphene Hybrid Nanosheets. *Energy Environ. Sci.* **2016**, *9*, 1430–1438.

(60) Li, X.; Sun, X.; Gao, Z.; Hu, X.; Ling, R.; Cai, S.; Zheng, C.; Hu, W. A Simple One-Pot Strategy for Synthesizing Ultrafine SnS_2 Nanoparticle/Graphene Composites as Anodes for Lithium/Sodium-Ion Batteries. *ChemSusChem* **2018**, *11*, 1549–1557.

(61) Yang, Z.; Zhang, P.; Wang, J.; Yan, Y.; Yu, Y.; Wang, Q.; Liu, M. Hierarchical Carbon@SnS_2 Aerogel with "Skeleton/Skin" Architectures as a High-Capacity, High-Rate Capability and Long Cycle Life Anode for Sodium Ion Storage. *ACS Appl. Mater. Interfaces* **2018**, *10*, 37434–37444.

(62) Kovtyukhova, N. I.; Ollivier, P. J.; Martin, B. R.; Mallouk, T. E.; Chizhik, S. A.; Buzaneva, E. V.; Gorchinskiy, A. D. Layer-by-Layer Assembly of Ultrathin Composite Films from Micron-Sized Graphite Oxide Sheets and Polycations. *Chem. Mater.* **1999**, *11*, 771–778.

For Table of Contents Only:

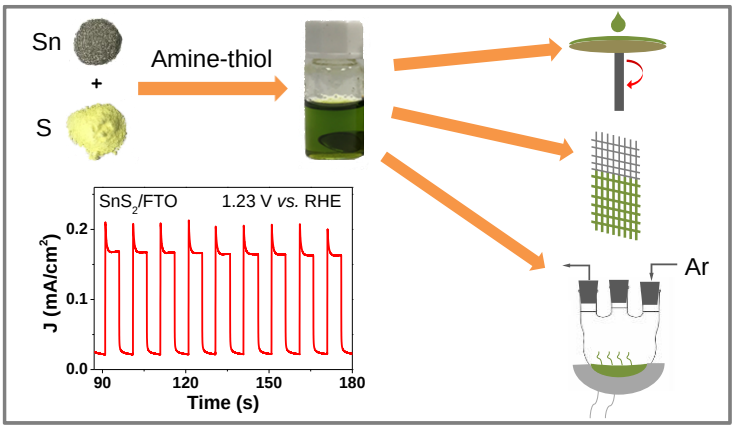
Sn
+
S
Amine-thiol
SnS2/FTO
1.23 V vs. RHE
J (mA/cm2)
0.0
0.1
0.2
90
120
150
180
Time (s)
Ar